

# Failure analysis of adhesively-bonded metal-skin-to-composite-stiffener: effect of temperature and cyclic loading

Sofia Teixeira de Freitas<sup>a,\*</sup>, Jos Sinke<sup>a</sup>

<sup>a</sup>*Delft University of Technology, Kluyverweg 1, 2629 HS Delft, The Netherlands*

---

## Abstract

The aim of this research is to analyse the failure of a Fiber Metal Laminate (FML) skin adhesively bonded to a Carbon Fiber Reinforced Polymer (CFRP) stiffener, under quasi-static loading at different environmental temperatures ( $-55^{\circ}\text{C}$ , Room Temperature RT and  $+100^{\circ}\text{C}$ ) and under fatigue loading at RT. This bonded joint was tested using stiffener pull-off tests, which is a typical setup used to simulate full-scale components subject to out-of-plane loading. The failure sequence for all test conditions consist of: (1) damage initiation at the noodle of the CFRP stiffener; (2) damage propagation by delamination from the noodle to the stiffener foot; (3) detachment of the stiffener from the skin. Increasing the temperature, decreases the joint stiffness (40% when compared to RT) and decreasing the temperature decreases the maximum load (50% when compared to RT). The fatigue life initiation of the joint presents a very large scatter but the fatigue life propagation presents more stable results. The fatigue threshold (no damage) is reached at approximately 30% of the maximum load level. The fracture surfaces indicate a predominant inter and intra-laminar failure of the composite under mixed mode I/II. The CFRP stiffener is the weakest link of the bonded FML-skin-to-CFRP-stiffener both for static and fatigue loading.

### *Keywords:*

Adhesive bonding, skin-to-stiffener connection, composite-to-aluminium joints, thermal loading, fatigue

---

\*Corresponding author: S.TeixeiraDeFreitas@tudelft.nl

## 1. Introduction

Since Boeing 787 and Airbus A350X have entered in service, composite materials officially claimed more than 50% of the structural weight of a commercial aircraft. However, in order to fully exploit the weight-savings potential of composite material in full-scale structures, a suitable joining technology must be implemented. Adhesive bonding offers major advantages for joining composites when compared to riveting or welding. Not only in terms of structural performance, since it avoids high stress concentrations, but also in the ability to join different materials. Though composites have become the number one material in the latest aircraft, the next generation might find the optimum efficiency by combining different types of materials, found to be the most suitable for the different structural components of an aircraft. Joining different materials will become then of major importance.

The research described in this paper focus on carbon fiber reinforced polymer stiffeners (CFRP) adhesively bonded to fiber metal laminate skins (FML). Skin-to-stiffener joints are common in the fuselage panels and in the wing panels of an airplane structure. In order to simulate the structural behavior of those full-scale structures, sub-component tests are performed which reproduce the load and boundary conditions. The Stiffener Pull-Off Test (SPOT) is a common sub-component test method to simulate out-of-plane loading in skin-to-stiffener joints, such as internal pressure on a fuselage panel or low pressure zones on leading edges [1–3]. Most of the existing research on skin-to-stiffener joints studies co-cured CFRP joints or metal-to-metal bonded joints [4–7]. No significant research has been performed in composite-to-metal structures.

Most of the research in composite-to-metal bonded joints is limited to coupon tests. Single- and double-lap joints (SLJ and DLJ) have been used to evaluate the shear strength of bonded composite-to-aluminium joints [8–10]. Double cantilever beam (DCB) hybrid specimens are used to characterize the crack propagation behavior and providing input data for fracture mechanics [11, 12]. Since adhesion is one of the key components for guaranteeing the integrity of bonded joints, floating roller peel tests have been adapted in order to assess the adhesion quality of composite-to-metal bonded joints [13, 14].

However in order to succeed, composite-to-metal bonded joints also need to prove their performance in sub-component applications, such as skin-to-stiffener joints.

The research presented in this paper is part of an experimental campaign on adhesively

bonded FML-skins-to-CFRP-stiffeners. In the work previously published by the authors [15], the metal-to-composite bonded joint was compared to metal-to-metal bonded joint. Static tests at Room Temperature (RT) were performed for both configurations. The study concluded that the failure mechanisms are significantly different. For the metal-to-metal bonded joint, the failure was mainly cohesive and very sudden, with limited damage tolerance. For the composite-to-metal bonded joint, the failure mainly occurred in the composite stiffener as inter- and intra-laminar failure. The composite-to-metal solution had significantly lower load carrying capacity (less 40% to 60%) than the metal-to-metal solution but the failure sequence yield to a more damage tolerant design than the former [15].

This paper presents the follow up of the previous research. The aim was, firstly, to study the effect of different environmental temperatures in the static behaviour of the metal-skin-to-composite-stiffener bonded joint, and, secondly, to study the fatigue behaviour of the same bonded joint at RT.

## 2. Materials and Specimens

Stiffener pull-off test specimens were manufactured by bonding a Carbon Fibre Reinforced Polymer (CFRP) stiffener to a Fiber Metal Laminate (FML) skin.

### 2.1. Materials

The Fiber Metal Laminate (FML) skin was Glare 5-3/2-0.3, which consists of three 2024-T3 aluminium alloy layers 0.3 mm thick, bonded together with glass prepregs S2-glass/FM-94 with the layup  $[0^\circ/90^\circ/90^\circ/0^\circ]$ . This layup is typical of Glare 5, which is generally used at location prone to impact loading [16]. The skin layup is therefore  $[Al/[0^\circ/90^\circ/90^\circ/0^\circ]/Al/[0^\circ/90^\circ/90^\circ/0^\circ]/Al]$ . The outer faces of the skin are Aluminium layers (metal). The skin was cured in the autoclave according to the standard procedure for Glare (4 bars, 60 min at 120 °C). The aluminium surfaces were pre-treated with chromic acid anodizing and primed with BR 127 (Cytec Engineered Materials, Tempe, Arizona, USA).

The CFRP stiffeners were prepared from unidirectional pre-preg consisting of HexPly 8552 epoxy matrix in combination with AS4 carbon fiber (Hexcel Corporation, Stamford, Connecticut, USA). The CFRP stiffener was an inverted T-shape stiffener. The web and flange of the CFRP foot have the same layup  $[+45^\circ/0^\circ/90^\circ/-45^\circ]_5$ . The noodle region (junction of the T-arms) was

filled with  $0^\circ$  fibers (stiffener's length direction). The layup was selected by the manufacturer of the T stiffeners, Fokker Aerostructures. The stiffener was cured at  $180^\circ\text{C}$  for 120 min in the autoclave. Prior to bonding, the CFRP-stiffener-foot surfaces were abraded with sand paper and then wiped clean with an acetone-soaked cloth. Figure 1 shows the configuration of the CFRP stiffener. The average thickness of the T-web was 1.43 mm (standard deviation of 2%) and of the T-flange was 1.54 mm (standard deviation of 3%).

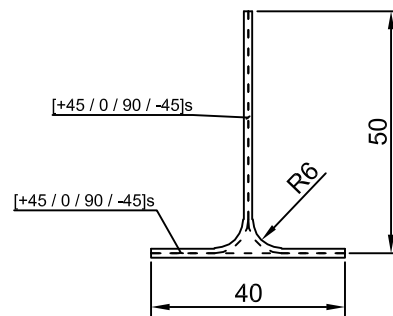


Figure 1: CFRP Stiffeners' configuration (dimension in mm).

Two structural adhesives were used – AF 163-2K.06 (3M, Minnesota, USA) and EA9696.060 PSF K (Henkel, Düsseldorf, Germany). Both are epoxy film adhesives with a curing temperature of  $120^\circ\text{C}$  for 90 min in the autoclave. These two adhesives had the best performance from screening tests performed on ten different adhesives, in terms of good adhesion to metals and to composites, and in terms of apparent average shear strength [14]. AF 163-2 has been on the market for many years and it is being used for metal bonding and, more recently, for composite bonding. EA 9696 is especially tailored for high toughness applications. This last feature can be of major importance for the hybrid joint, since we are joining materials with different coefficient of thermal expansion.

Tables 1 and 2 show the mechanical properties taken from literature and from the Technical Data Sheet (TDS) of the materials used. According to the manufacturers data, the Glass transition temperature ( $T_g$ ) of the adhesives AF 163-2 and EA 9696 is approximately  $+110^\circ\text{C}$  and the  $T_g$  of the epoxy resin FM94 of the glass prepeg is approximately  $+100^\circ\text{C}$ .

Table 1: Mechanical properties of the isotropic materials used.

	$E$ (MPa)	$\sigma_y$ (MPa)	$\sigma_{max}$ (MPa)	$\nu$
Al 2024-T3	72400	347	420	0.33
AF 163-2 (TDS)	1110	–	48.3	0.34
EA 9696 (TDS)	2082	–	45.9	0.34

Table 2: Mechanical properties of the orthotropic materials used.

	$E_1$ (MPa)	$E_2$ (MPa)	$\nu_{12}$	$\nu_{21}$
S2-glass/FM-94	48900	5500	0.33	0.0371
HexPly-8552/AS4 (TDS)	131000	9240	0.302	0.029

## 2.2. Specimens

The base line of the Pull-off specimens is a Glare skin adhesively bonded to a CFRP stiffener at mid length. Two series of specimens were manufactured, one using AF 163-2 and another using EA9696. The specimens were 100 mm wide and 200 mm long.

## 3. Experimental Procedure

### 3.1. Adhesive material testing

Tensile tests were performed on the adhesives bulk material at three environmental temperatures:  $-55^\circ\text{C}$ , room temperature ( $+22^\circ\text{C}$ ) and  $+100^\circ\text{C}$ . Adhesive films without carrier were used to manufacture dog-bone shaped specimens – AF163-2U.015WT and EA9696.060 NW. The experimental procedure and specimens dimensions were in accordance with the standard ASTM D638 [17]. A temperature chamber was coupled to the testing machine to test under different temperatures (temperature accuracy  $\pm 2^\circ\text{C}$ ). The tests were carried out at displacement control at a testing speed of 5 mm/min using a testing machine with a load cell of 10 kN. Five specimens were tested in each test series. A mechanical extensometer was used to measure the specimens' elongation.

### 3.2. Stiffener pull-off tests

The pull-off test setup is shown in Figure 2. The clamping of the skin was guaranteed by two steel plates on each support, connected to the skin by bolts. A vertical tensile load was applied

to the stiffener web (P – see Fig. 2) using a clamp. The skin span was constant for all test series and equal to 100 mm.

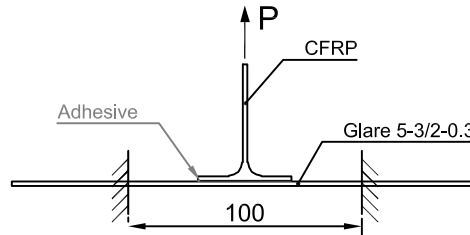


Figure 2: Experimental setup (dimension in mm).

### 3.2.1. Quasi-static tests

The quasi-static tests were performed at three environmental temperatures:  $-55^{\circ}\text{C}$ , room temperature ( $+22^{\circ}\text{C}$ ) and  $+100^{\circ}\text{C}$ . A temperature chamber was coupled to the testing machine in order to test at high and low temperatures. The tests were carried out at displacement control at a testing speed of 3mm/min. The loads and piston displacement were recorded during testing. The tests were performed until the stiffener was completely detached from the skin. Typically, three specimens were tested at the same test conditions.

### 3.2.2. Fatigue tests

Fatigue tests were performed at room temperature. The maximum load levels were in the range from 60% to 30% of the maximum load of the correspondent quasi-static tests. The tests were carried out in load control with a constant applied load ratio  $R = 0.1$  ( $R = P_{\min}/P_{\max}$ ). A sinusoidal wave form at 5 Hz frequency was used.

## 4. Results and Discussion

### 4.1. Adhesive material testing

Figure 3 shows representative stress-strain curves of the adhesives AF163-2 and EA9696. Table 3 lists the tensile mechanical properties for both adhesives at the three temperatures tested – Young's modulus  $E$ , tensile strength  $\sigma_{\max}$  and tensile failure strain  $\epsilon_{\max}$ .

The increase of temperature results in a decrease of tensile strength and material stiffness while the maximum strain increases. Both at RT and at +100 °C, the adhesive EA9696 is more ductile than the adhesive AF 163-2 (the maximum strain is higher in the former than in the latter), while the tensile strength remains similar between the two adhesives. At -55 °C both adhesives show brittle behaviour but AF163-3 tensile strength is 45% higher than EA9696.

At room temperature, the results of the tensile tests are in agreement with the values obtained from literature (see Table 1) with the exception of the Young’s modulus of AF163-2. The value from the tensile tests is 80% higher than the one given at the Technical Data Sheet (Table 3 AF163-3 (tests) –  $E_{RT} = 2043$  MPa and Table 1 AF 163-2 (TDS) –  $E_{RT} = 1110$  MPa). Nevertheless, the tests results have a significant confidence since within the 5 specimens tested only 6% of standard deviation was observed from the average value 2043 MPa.

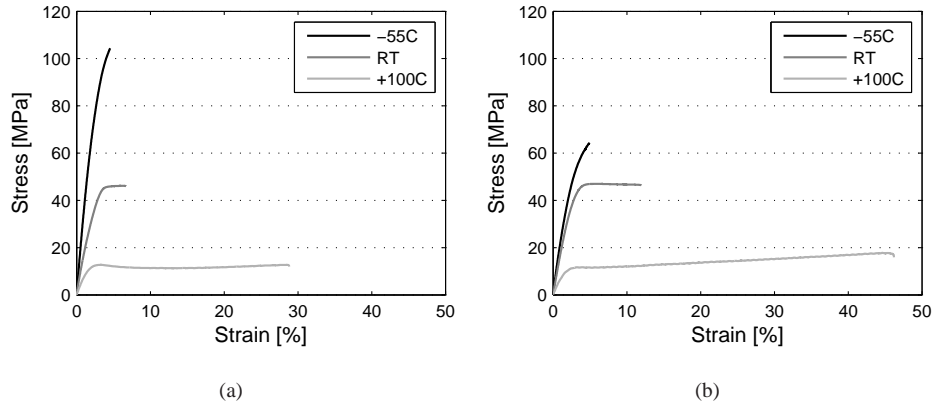


Figure 3: Tensile stress-strain curves of adhesive (a) AF163-2 and (b) EA9696.

Table 3: Tensile mechanical properties of AF163-3 and EA9696 (average  $\pm$  relative standard deviation).

	AF 163-2			EA9696		
	$E$ (MPa)	$\sigma_{max}$ (MPa)	$\epsilon_{max}$ (%)	$E$ (MPa)	$\sigma_{max}$ (MPa)	$\epsilon_{max}$ (%)
-55 °C	$3085 \pm 14\%$	$102.90 \pm 6\%$	$4.81 \pm 14\%$	$2505 \pm 4\%$	$70.50 \pm 7\%$	$4.49 \pm 14\%$
RT	$2043 \pm 6\%$	$45.70 \pm 3\%$	$5.38 \pm 27\%$	$2019 \pm 4\%$	$47.83 \pm 2\%$	$11.51 \pm 14\%$
+100 °C	$683 \pm 17\%$	$12.97 \pm 8\%$	$29.45 \pm 30\%$	$999 \pm 5\%$	$19.85 \pm 9\%$	$56.79 \pm 16\%$

#### 4.2. Quasi-static stiffener pull-off tests

Typical load-displacement curves at the tested three temperatures for the two adhesive are shown in Figure 4(a), and the correspondent failure sequence in Figure 4(b). The damage typically initiated at the noodle region of the CFRP stiffener (point 1 in Figure 4), corresponding to the maximum pull-off load registered. This damage initiation is accompanied by a sudden drop of the load, from which the damage propagates at much lower load levels, approximately 40% of maximum load (point 2 in Figure 4). The initial crack propagated through the stiffener foot plies and through the web plies. The damage sequence was very similar within the temperature range tested and for the two adhesives.

The final failure occurs when the composite stiffener is completely detached from the skin. A typical final fracture surface is shown in Fig. 5 and clearly shows interlaminar and intralaminar failure of the composite. Furthermore, from the fracture surface and from the damage propagation, one can also observe that the crack tends to propagate through the symmetry plane of the layup of the stiffener  $[+45^\circ/0^\circ/90^\circ/-45^\circ]_S$  and between the  $-45^\circ$  and  $90^\circ$  plies.

There was no failure observed in the adhesive bondline for any of the specimens tested. Even when the thermal residual stresses are maximum at the bondline (at  $-55^\circ\text{C}$ ), damage still occurs in the composite stiffener and not in the adhesive. These results show that both adhesives AF 163 and EA9696 are ductile enough to withstand the thermal residual stresses induced at the bondline due to considerably different coefficients of thermal expansion between the CFRP stiffener and the Glare skin. It can be considered that these residual stresses are zero at the curing temperature of the adhesive (at  $+120^\circ\text{C}$ ) and have their maximum value at  $-55^\circ\text{C}$  (largest temperature variation).

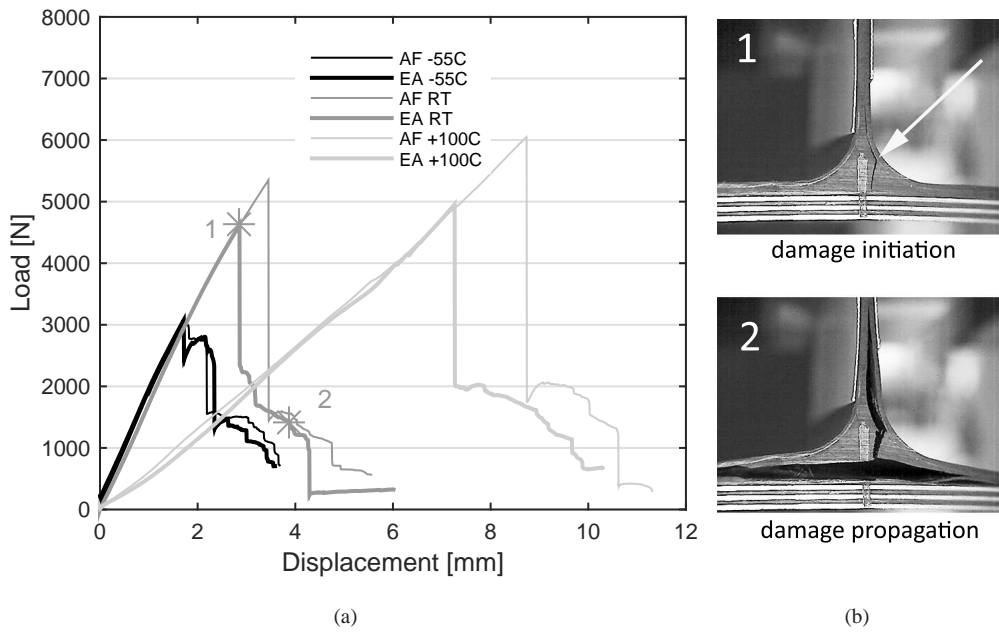


Figure 4: Typical load-displacement curves at the three temperatures tested for the two adhesives (a) and correspondent failure sequence for EA9696 RT test series (b) (the grey line crossing the stiffener noodle and the FML skin was drawn with a pen marker to identify the middle of the specimen).

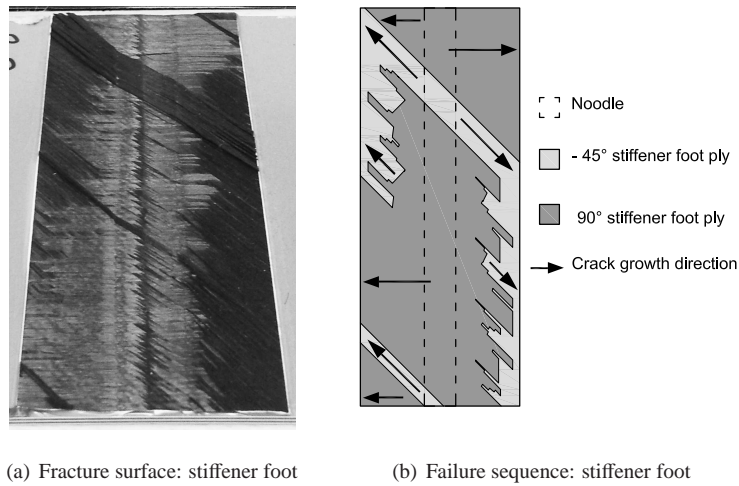


Figure 5: Typical fracture surfaces and failure sequence for static loading under the complete temperature range (-55 °C up to +100 °C).

Table 4 lists the test results including elastic flexural stiffness  $K$  ( $P/\delta$ ), maximum load  $P_{max}$  and displacement at maximum load  $\delta_{P_{max}}$  for the six test series (3 temperatures x 2 adhesives). The results for flexural stiffness  $K$  and maximum load  $P_{max}$  are also shown in Figure 6 in the format of a bar chart.

The maximum load and the corresponding displacement significantly increase with temperature. At +100 °C the maximum load increases approximately 15% to 30% when compared to RT. For the displacement the difference is even greater with more than twice the value for +100 °C when compared to RT. At -55 °C the maximum load and correspondent displacement decrease approximately 50% to 60% when compared to RT.

The flexural stiffness shows a different behaviour. At -55 °C and RT, the flexural stiffness are practically the same. However, at +100 °C, this value decreases almost 40% when compared to RT, as shown in Fig.6(b). The flexural stiffness of the tests corresponds to the flexural stiffness of the Glare skin. It has no influence of the adhesive material (same results independent of the adhesive used). The reason behind the significant drop of flexural stiffness at +100 °C, has to do with the fact that the resin of the glass prepreg layer used in the GLARE skin has a glass transition temperature close to +100 °C. At the glass transition temperature, the stiffness of the epoxy resin decreases significantly.

The increase of failure load with temperature has probably to do with the change of the mechanical behaviour of the composite stiffener with temperature, since that is where the failure occurs. As the behaviour of carbon fibers are not significantly affected by temperature within the range tested, the change in the mechanical behaviour of the composite stiffener must be caused by the temperature effect on the composite resin. The composite resins are epoxies, therefore the tensile tests performed on the adhesives, which are also epoxies, can give an indication of the temperature effect on those materials. As observed in Fig.3, epoxies show a brittle behaviour at low temperatures and ductile behaviour at high temperatures. The increase of ductility of the epoxy resin in the composite results in a decrease of stress concentration at the stiffener. The decrease of stress severity postpones the damage initiation at the central noodle and increases the maximum load and the corresponding displacement.

The significant decrease of flexural stiffness of the skin at 100 °C also contributes to a better load distribution in the joint, contributing for less stress concentration and higher load capacities than at lower temperatures.

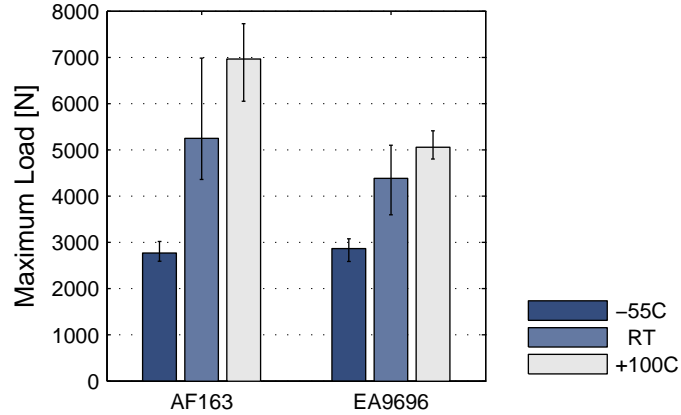
No influence of the adhesive (AF163 vs. EA 9696) is observed neither in the maximum load values nor in the flexural stiffness.

Table 4: Stiffener pull-off test results: stiffness  $K$ , maximum load  $P_{max}$  and displacement at maximum load  $\delta_{P_{max}}$  (average  $\pm$  relative standard deviation).

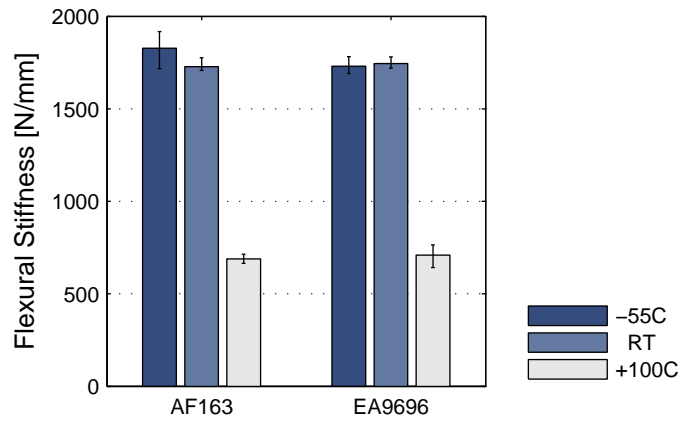
	AF 163-2			EA9696		
	$K$ (N/mm)	$P_{max}$ (N)	$\delta_{P_{max}}$ (mm)	$K$ (N/mm)	$P_{max}$ (N)	$\delta_{P_{max}}$ (mm)
-55 °C	1827 $\pm$ 6%	2769 $\pm$ 8%	1.7 $\pm$ 9%	1730 $\pm$ 3%	2867 $\pm$ 9%	1.8 $\pm$ 5%
RT	1727 $\pm$ 2%	5249 $\pm$ 20%	3.3 $\pm$ 22%	1745 $\pm$ 2%	4386 $\pm$ 16%	2.7 $\pm$ 16%
+100 °C	689 $\pm$ 5%	6963 $\pm$ 12%	8.2 $\pm$ 9%	709 $\pm$ 9%	5058 $\pm$ 6%	7.3 $\pm$ 6%

#### 4.3. Fatigue stiffener pull-off tests

Under cyclic loading, the typical damage evolution is similar to the one observed under quasi-static loading. The damage occurs entirely in the CFRP stiffener. Figure 7 shows the typical fatigue damage events observed. The fatigue crack initiates at the stiffener noodle at the same location as presented in the quasi-static tests – see Figure 7(b). The number of cycles from the starting of the tests up to crack initiation is here referred to as *fatigue life initiation* and by the symbol  $n_i$ . After initiation, the fatigue damage propagates through the CFRP stiffener foot plies and web plies – see Figure 7(c). Finally, there is a complete detachment of the stiffener from the skin – see Figure 7(d). The number of cycles from the crack initiation up to the final detachment is referred to as *fatigue life propagation* and by the symbol  $n_f$ . These fatigue damage events can also be identified in the displacement values measured during the fatigue tests. Three examples of the displacement versus number of cycles are shown in Figure 8. The mean values are determined by  $0.5 \cdot (\delta_{max} + \delta_{min})$  and the range values by  $|\delta_{max} - \delta_{min}|$ . In specimen 1, with the highest load level (60% – see Figure 8(a)), there is a steep increase of the displacement when the final failure occurs at the very end of the test. No damage has been observed before that. The slight increase in the displacement values measured from the beginning of the test is related with the progressive fitting of the specimen to the clamping of the test set up. In this example, the damage event is very sudden and the crack initiation and final failure occur almost simultaneously. The *fatigue life propagation* is hence zero ( $n_f = 0$ ). In specimen 2 and 3, both with 40% load level – see Figures 8(b) and 8(c), the crack initiation and the final failure can be distinctively identified. In



(a)



(b)

Figure 6: Maximum load (a) and flexural stiffness (b) at the three temperatures tested for the two adhesives.

both cases, the crack initiation is followed by an increase in the displacement, especially visible at the mean value. The number of cycles up to this point is the *fatigue life initiation*, point  $n_i$ . From this point the crack propagates up to the final failure identified by the steep increase in the displacement values (point  $n_i + n_f$ ). The number of cycles from the initiation up to the final failure is the *fatigue life propagation*,  $n_f$ . Finally, no disbond was detected in the bondline nor delamination in the FML skin in none of the fatigue tests.

Table 5 presents the results of the fatigue life initiation and propagation ( $n_i$  and  $n_f$ ) for the complete test series. The same results are presented in Figure 9 where  $n_i$  and  $n_f$  are plotted

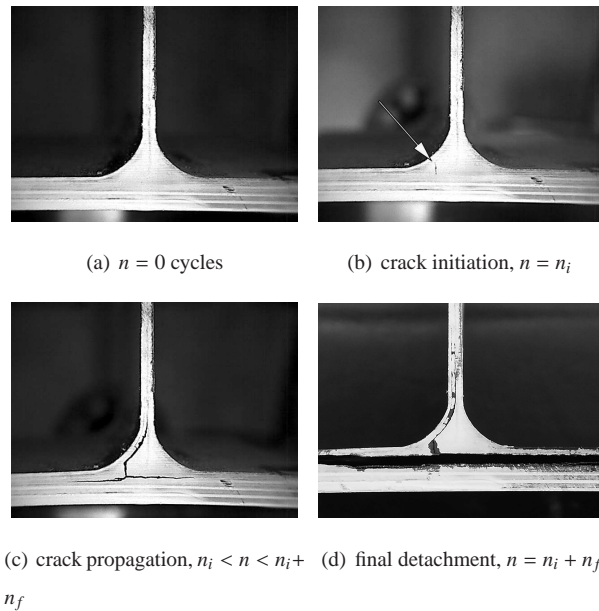


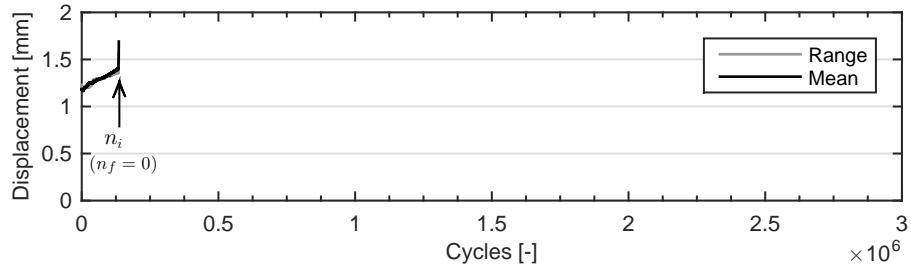
Figure 7: Typical fatigue damage events ( $n$ –number of fatigue cycles;  $n_i$ – number of cycles to crack initiation – *fatigue life initiation*;  $n_f$ – number of cycles from crack initiation to complete detachment – *fatigue life propagation*).

against the maximum fatigue load  $P_{max}$ , Figure 9(a) and 9(b), respectively.

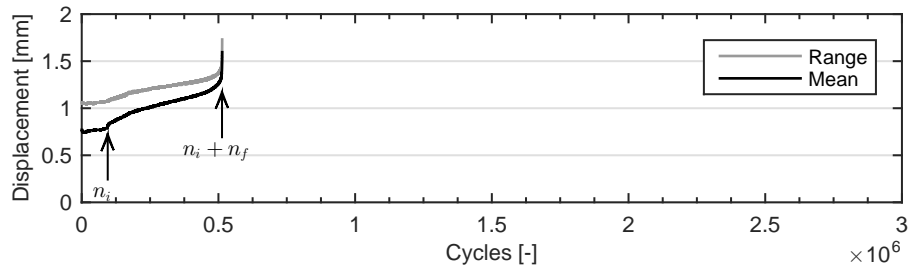
A total of 14 specimens were tested under cyclic loading, six with adhesive AF163-2 and eight with adhesive EA9696.

In the AF163-2 series, the test carried out at 60% of the maximum load level had a fatigue life initiation at  $1.35e+05$  cycles. This is the same specimen as shown previously in Figure 8(a) where the final failure occurred almost simultaneously with the crack initiation ( $n_f = 0$ ). Three tests were carried out at the 40% load level. The fatigue life initiation presents significant scatter at this load level, from  $1e+05$  up to  $2.35e+06$  cycles – see Figure 9(a). However, the fatigue life propagation values of the same specimens present less scatter, with values between  $2.0e+05$  and  $4.0e+05$  cycles – see Figure 9(b). On the two fatigue tests carried out at 30% of the load level, no damage was detected until  $2.5e+06$  cycles (run out initiation).

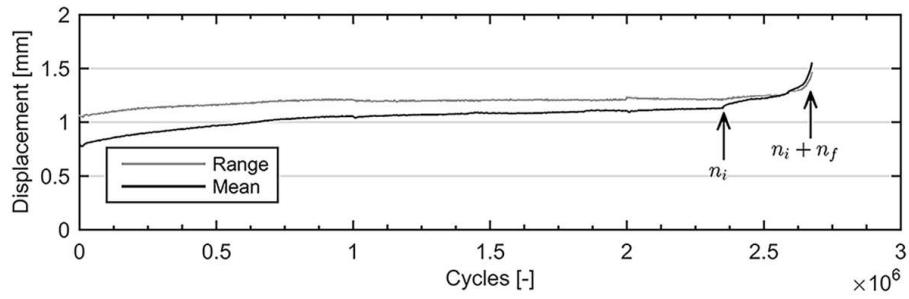
In the EA9696 series, on the two tests carried out at 60% of the load level, the crack initiation occurred between  $2.5e+04$  and  $2.0e+05$  cycles – see Figure 9(a). The values of fatigue life propagation present less scatter than the ones for fatigue life initiation, with values between  $1.6e+04$  and  $4.6e+04$  – see Figure 9(b). Four tests were carried out at 40% load level. The fatigue life



(a) Specimen 1 ( $60\% P_{max-static}$ )

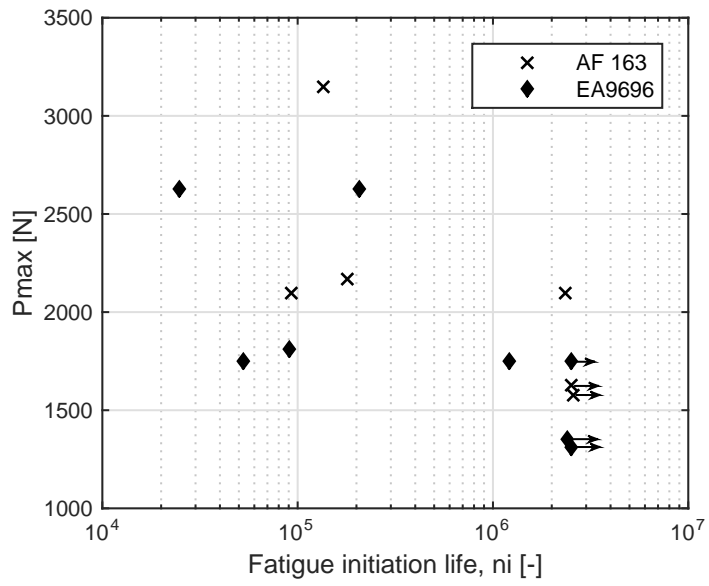


(b) Specimen 2 ( $40\% P_{max-static}$ )

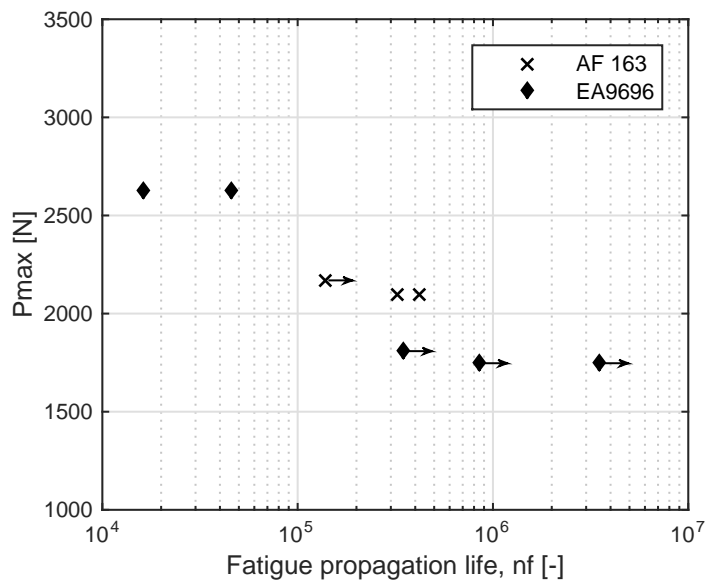


(c) Specimen 3 ( $40\% P_{max-static}$ )

Figure 8: Displacement versus number of cycles recorded during three fatigue tests.



(a)



(b)

Figure 9: Fatigue life.

Table 5: Stiffener pull-off fatigue test results (*run out initiation* - no crack initiation; *run out propagation* - crack initiation but no final failure).

	$P_{max}/P_{max-static}$	$P_{max}$ (N)	$P_{min}$ (N)	$n_i$ (cycles)	$n_f$ (cycles)	
AF 163	0.60	3150	315	1.35E+05	0	spec.1 Fig.8(a)
	0.40	2100	210	9.30E+04	4.21e+05	spec.2 Fig8(b)
	0.41	2170	232	1.80E+05	>1.40E+05	run out propagation
	0.40	2100	209	2.35E+06	3.26E+05	spec.3 Fig.8(c)
	0.31	1625	179	>2.50E+06	–	run out initiation
	0.30	1575	158	>2.58E+06	–	run out initiation
EA 9696	0.60	2630	263	2.50E+04	4.55e+04	
	0.60	2630	263	2.07E+05	1.62E+04	
	0.40	1754	175	5.32E+04	>8.47E+05	run out propagation
	0.41	1811	190	9.00E+04	>3.48E+05	run out propagation
	0.40	1754	175	1.20E+06	>3.50E+06	run out propagation
	0.40	1754	175	>2.54E+06	–	run out initiation
	0.31	1351	142	>2.43E+06	–	run out initiation
	0.30	1316	132	>2.50E+06	–	run out initiation

initiation values have again a significant scatter, two specimens before  $1e+05$  cycles, one specimen at  $1.2e+06$  cycles and finally a run out initiation until  $2.5e+06$  cycles. The three specimens where the crack did initiate, the tests were stopped before final failure (run out propagation). Finally, at 30% load level, the two specimens did not present any damage until  $2.5e+06$  cycles (run out initiation).

For the complete test series, the fatigue life initiation values present a very large scatter – see Figure 9(a). This might be related with the fact that, the damage initiates at the CFRP stiffener noodle, where the level of stress concentration may present a significant scatter due to small initial manufacturing defects at that location. The stiffener noodle is prone to manufacturing defects due to the complexity of layup at that area and a possible lack of pressure in the region of the curvature between the web and the foot. Moreover, residual stresses are also present in this area since the noodle is filled with long  $0^\circ$  fibers which induce residual thermal stresses in the matrix when cooling down the CFRP stiffener and, therefore, can yield to early matrix failure.

The fatigue life propagation presents more stable results, with less scatter in the same load

level, than the fatigue life initiation. This indicates that, although the crack initiation is unstable, the crack propagation is stable which allows for a good prediction of the fatigue life propagation and a steady damage tolerant design. It is known that damage tolerance uses fracture mechanics concepts, through the determination of crack growth equations based on crack modes (I to II). It is then important to analyze the characteristics of the crack growth through fractographic analysis which will be explained in the next section.

For a safe-life design (no crack initiation), the fatigue threshold of this bonded structures is in the vicinity of 1200 N to 1500 N pull-off load, corresponding to 30% of maximum load level.

The results show that the noodle of CFRP stiffener is the weakest spot of the bonded structure. The fatigue damage did not occur at the adhesive bondline and therefore the influence of the type of adhesive used in this study in the damage progression is not significant. A re-design of the CFRP stiffener, and especially of the noodle region, might bring significant improvements on the performance of the bonded structure and decrease the scattered fatigue behaviour.

## **5. Fractographic analysis**

In this section the effect of temperature and cyclic loading on the fracture morphology of the composite-to-metal bonded joint will be discussed. This analysis will help to identify if the environmental temperatures and cyclic loading influence the failure mechanism of the joint. The analysis consisted in, firstly, visually observe the exposed fracture surfaces, secondly, select areas of interest using optical microscopy and finally, fully characterize the fracture surfaces using Scanning Electron Microscope (SEM).

The analysis was performed at two crack locations: Location 1 at the area of crack initiation at the CFRP stiffener noodle; Location 2 at the area of crack propagation at the CFRP stiffener foot plies – see Figure 10.

Table 6 show typical pictures taken at the location of crack initiation (Location 1) for the 4 test series: static at  $-55^{\circ}\text{C}$ , RT,  $+100^{\circ}\text{C}$  and fatigue at RT.

Morphology features typical of mixed mode I/II delamination can be identified. In the resin rich areas, shallow cusps can be identified for all the test conditions. These shear cusps are less steep than commonly identified in pure mode II due to the presence of mode I loading. Previous research shows that the lower the mode mixity I/II, the steeper are the shears cusps [18, 19]. This may justified why along the fracture surfaces some cusps were more shallow than others

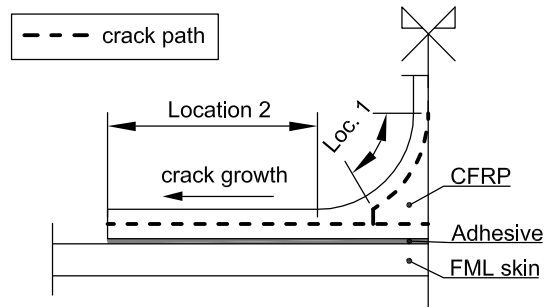


Figure 10: Locations of the fractographic analysis along the crack path.

depending on the mode mixity on that particular location. Looking to the particular morphology of these shallow cusps, at  $-55^{\circ}\text{C}$  the cusps present “serrated feet”. This is a particular feature of mixed mode delamination. It consists of microcracks developed at the edges of the cusps which converge as the center of the cusp approaches [18]. As the temperature increases, the serrated feet vanishes. At  $+100^{\circ}\text{C}$  no serrated feet at the edges of the cusps can be identified. The increase of ductility of the matrix of the CFRP with temperature has a clear effect on the cusps morphology: edges become smoother and the cusps become more flake-like (less serrated feet).

The fracture surface at the crack initiation due to fatigue loading looks very much alike the fracture surface of the static loading at the same location. Shallow cusps can be as well identified indicating that mixed mode I/II delamination is the main failure mechanism for crack initiation under fatigue. The similarity in the fractures surfaces between static and fatigue loading indicate that very similar failure mechanics are involved in the crack initiation under both loads.

Table 7 compares the typical fracture morphologies at the CFRP stiffener foot plies at different temperatures under static loading (Location 2). These pictures represent the typical fracture surfaces found along the complete path of the crack propagation – the complete length of the CFRP stiffener foot plies. Again features of mixed mode I/II delamination can be identified, such as shallow cusps. As the temperature increases the fracture surface gets less rough and more smooth. The pictures shown with amplification 5.0k show clearly the changes in morphology of the cusps with temperature: serrated feet at  $-55^{\circ}\text{C}$  and flakes-like cusps with smooth edges at  $+100^{\circ}\text{C}$ .

Table 6: Typical static and fatigue fracture surfaces at Location 1: crack initiation – stiffener noodle (x1k).

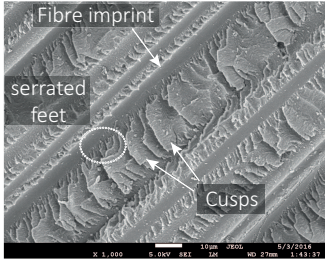
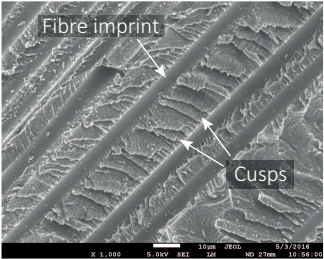
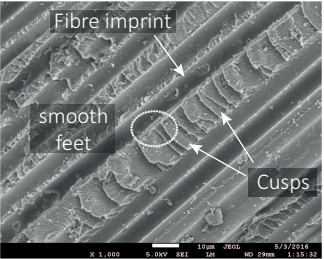
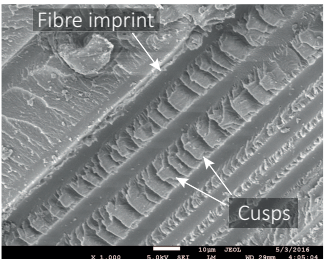
Load	-55 °C	RT	+100 °C
Quasi-static			
Fatigue	–		–

Table 7: Typical static fracture surfaces at Location 2: crack propagation – stiffener foot plies.

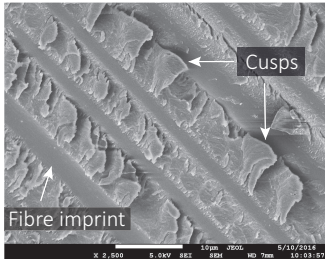
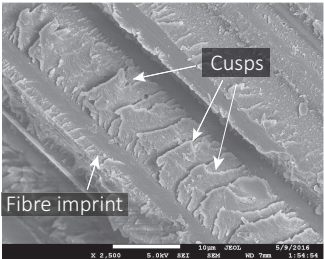
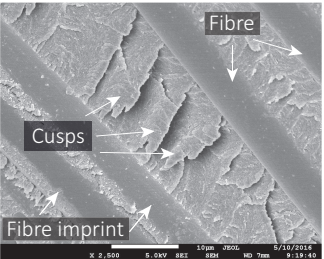
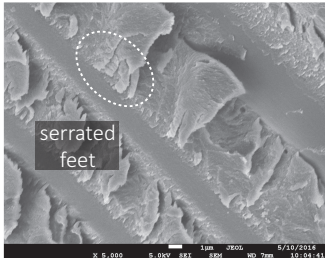
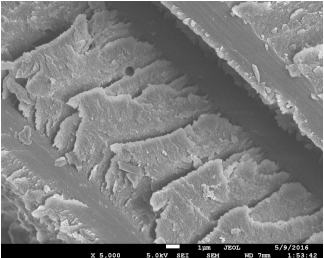
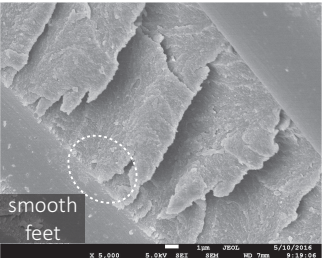
Scale	-55 °C	RT	+100 °C
x2.5k			
x5.0k			

Figure 11 compares two fracture surfaces of quasi-static and fatigue loading at the location 2 - crack propagation, on the fibre imprint side. The fatigue fracture surface presents less roughness and more debris in comparison with the static fracture surface. Moreover, cups are not so easily distinguishable nor as frequent in the fatigue as in the static surface.

Figure 12 shows fracture surfaces under fatigue loading at the same location but now at the fibre side. The cusps under fatigue loading tend to be rolled and less steep than in the quasi static loading. This leads to less distinguished cups in the fibre imprint side presented in Figure 12. According to literature [18], the rolling of the matrix becomes more apparent with increasing the mode II in a mixed mode interlaminar failure. The presence of cusps identifies mix-mode I/II delamination as the typical failure mechanism under fatigue crack propagation.

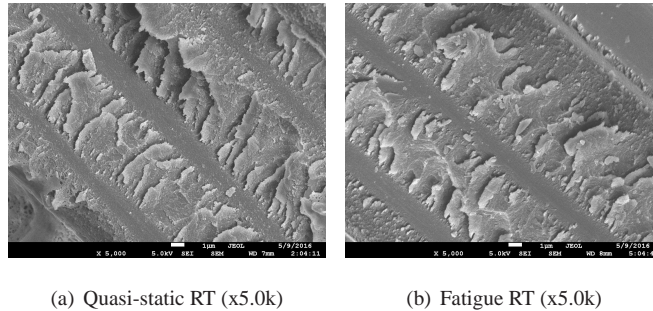


Figure 11: Fracture surface at Location 2: crack propagation at the fibre imprint side

## 6. Conclusions

Stiffener pull-off tests were performed on adhesively bonded FML-skin-to-CFRP-stiffeners. Quasi-static tests were performed at three environmental temperatures  $-55^{\circ}\text{C}$ , RT and  $+100^{\circ}\text{C}$ , and fatigue tests were performed at RT. Two types of epoxy film adhesives were used AF163-2 and EA9696. The aim was to analyze the fracture mechanism and failure sequence of composite-to-metal bonded structure under temperature and fatigue.

From the analysis of the tests, the following conclusions can be drawn:

- The quasi-static damage sequence is very similar within the temperature range tested and for the two adhesives. The damage initiates at the central noodle of the composite stiffener. The initial damage corresponds with the maximum load. Unstable delamination

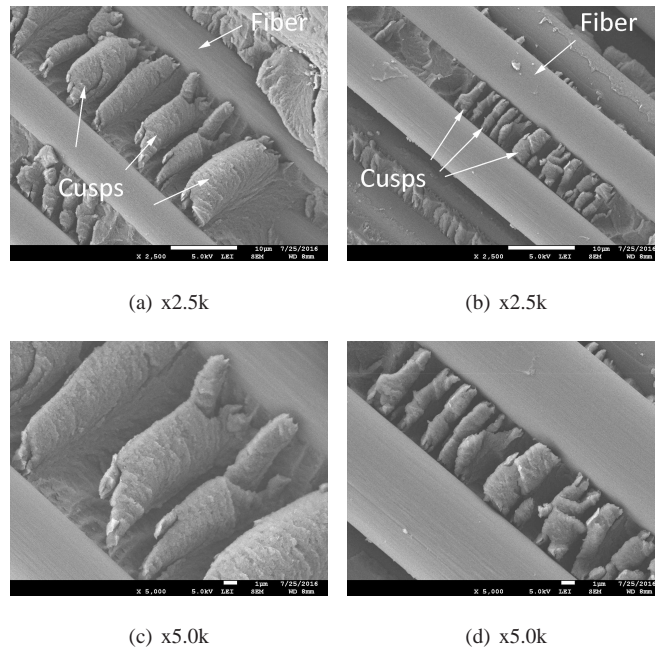


Figure 12: Fatigue fracture surfaces at Location 2: crack propagation, at the fibre side – stiffener foot plies.

then propagates from the noodle to the tip of the stiffener foot at much lower load level (approximately 40% of maximum load).

- The quasi-static final failure occurs when the composite stiffener is detached from the skin. The failure mode is interlaminar and intralaminar failure of the composite, mainly in the stiffener foot plies.
- The stiffness of the composite-to-metal bonded structure is determined by the Glare skin flexural stiffness. A significant stiffness drop is observed when the testing temperature is close to the glass transition temperature of the epoxy resin of Glare’s glass-prepreg.
- The maximum load capacity of the joint increases with temperature due to an increase on the ductility of the composite stiffener and Glare skin. This allows for lower stress concentrations at “hot-spots”, such as the central noodle, allowing for higher maximum loads.
- The damage initiation and propagation is similar under quasi-static loading and fatigue loading. The crack initiates at the CFRP stiffener noodle and propagates through the CFRP

stiffener foot plies and web plies.

- No disbond was detected at the bond line in any of the quasi-static nor fatigue test, even at  $-55\text{ }^{\circ}\text{C}$  where high residual thermal stresses are expected at the adhesive bondline. Hence, for the type of adhesives tested, there was no significant influence on the fatigue behavior of the bonded structures.
- The fatigue life initiation of the bonded structures presents a very large scatter. The stress level at the stiffener noodle may present a significant scatter due to initial manufacturing defect yielding to a scatter in the crack initiation. Nevertheless, the fatigue life propagation presents more stable results which may allow for a good prediction and a damage tolerant design.
- The fatigue threshold of the bonded structure (no growth until 2.5 million cycles) is approximately at 30% of the maximum static pull-off load.
- the main failure mechanism undergoing at the CFRP stiffener is mixed mode I/II delamination, both under static and fatigue loading. The fracture morphology indicates that the mechanics of crack initiation are the same under static and fatigue loading.
- Flake-like shear cusps are a typical feature in the fracture surface of mix mode I/II delamination at high temperatures (above RT), opposite to cusps with serrated feet at lower temperatures. Under fatigue loading at the crack propagation area, the typical fracture morphology are rolled cusps.
- This research identifies that the composite stiffener is the weakest link of the composite-to-metal bonded structures in study, and not at the adhesive bondline. This holds for static loading in a wide temperature range and fatigue loading.

### **Acknowledgments**

This research was supported by Materials innovation institute (M2i) and Fokker Aerostructures.

## 7. References

- [1] P. Minguet, Analysis of the strength of the interface between frame and skin in a bonded composite fuselage panel, in: 38th AIAA/ASME/ASCE/AHS/ASC Structures, Structural Dynamics, and Materials Conference and AIAA/ASME/AHS Adaptive Structures Forum: A Collection of Technical Papers, 1997, pp. 2783–2790.
- [2] J. Li, T. K. O'Brien, C. Q. Rousseau, Test and Analysis of Composite Hat Stringer Pull off Test Specimens, *Journal of the American Helicopter Society* 42 (4) (1997) 350–357.
- [3] J. Li, Pull-off tests and analysis of composite skin and frame T-joint, in: 17th Technical Conference of the American Society for Composites, 2002, pp. 1–10.
- [4] E. Greenhalgh, M. H. Garcia, Fracture mechanisms and failure processes at stiffener run-outs in polymer matrix composite stiffened elements, *Composites Part A: Applied Science and Manufacturing* 35 (12) (2004) 1447–1458.
- [5] E. Greenhalgh, A. Lewis, R. Bowen, M. Grassi, Evaluation of toughening concepts at structural features in CFRP-Part I: Stiffener pull-off, *Composites Part A: Applied Science and Manufacturing* 37 (10) (2006) 1521–1535.
- [6] D. D. Cartié, G. DellAnno, E. Poulin, I. K. Partridge, 3D reinforcement of stiffener-to-skin T-joints by Z-pinning and tufting, *Engineering Fracture Mechanics* 73 (16) (2006) 2532–2540.
- [7] M. Demir Aydin, S. Akpınar, The strength of the adhesively bonded T-joints with embedded supports, *International Journal of Adhesion and Adhesives* 50 (2014) 142–150.
- [8] J. Owens, P. Lee-Sullivan, Stiffness behaviour due to fracture in adhesively bonded composite-to-aluminum joints II. experimental, *International Journal of Adhesion and Adhesives* 20 (1) (2000) 47–58.
- [9] S. Kang, M. Kim, C. Kim, Evaluation of cryogenic performance of adhesives using composite-aluminum double-lap joints, *Composite Structures* 78 (3) (2007) 440 – 446.
- [10] M. Seong, T. Kim, K. Nguyen, J. Kweon, J. Choi, A parametric study on the failure of bonded single-lap joints of carbon composite and aluminum, *Composite Structures* 86 (13) (2008) 135 – 145.
- [11] K. Ishii, M. Imanaka, H. Nakayama, Fatigue crack propagation behavior of adhesively-bonded CFRP/aluminum joints, *Journal of Adhesion Science and Technology* 21 (2) (2007) 153–167.
- [12] M. Khoshnavan, F. A. Mehrabadi, Fracture analysis in adhesive composite material/aluminum joints under mode-I loading: experimental and numerical approaches, *International Journal of Adhesion and Adhesives* 39 (2012) 8–14.
- [13] S. Teixeira de Freitas, J. Sinke, Adhesion properties of bonded composite-to-aluminium joints using peel tests, *The Journal of Adhesion* 90 (5-6) (2014) 511–525.
- [14] S. Teixeira de Freitas, J. Sinke, Test method to assess interface adhesion in composite bonding, *Applied Adhesion Science* 3 (1) (2015) 1–13.
- [15] S. Teixeira de Freitas, J. Sinke, Failure analysis of adhesively-bonded skin-to-stiffener joints: Metalmetal vs. compositemetal, *Engineering Failure Analysis*.
- [16] J. W. G. Ad Vlot, *Fibre Metal Laminates: An Introduction*, Kluwer Academic Publishers, The Netherlands, 2001.
- [17] ASTM-D638, D638-08: Standard Test Method for Tensile Properties of Plastics (2008).
- [18] E. Greenhalgh, *Failure analysis and fractography of polymer composites*, Woodhead Publishing Limited, UK, 2009.
- [19] R. Marat-Mendes, M. de Freitas, Fractographic analysis of delamination in glass/fibre epoxy composites, *Journal of Composite Materials* 47 (12) (2012) 1437–1448.